

Production of high-energy γ rays in proton- and α -induced reactions

Debasish Mondal,^{1,*} S. Mukhopadhyay^{1,2}, Deepak Pandit,^{1,2} Surajit Pal,¹ Pratap Roy^{1,2,†}, Balaram Dey,³ Srijit Bhattacharya⁴, A. De,⁵ Soumik Bhattacharya,¹ K. Banerjee^{1,2}, S. Kundu,¹ S. Manna,^{1,2} T. K. Rana,^{1,2} R. Pandey,¹ S. R. Banerjee¹ and C. Bhattacharya^{1,2}

¹Variable Energy Cyclotron Centre, 1/AF-Bidhannagar, Kolkata 700064, India

²Homi Bhabha National Institute, Training School Complex, Anushaktinagar, Mumbai 400094, India

³Department of Physics, Bankura University, Bankura 722155, India

⁴Department of Physics, Barasat Government College, Barasat, North 24 Parganas, Kolkata 700124, India

⁵Department of Physics, Raniganj Girls' College, Raniganj 713358, India

 (Received 23 November 2021; revised 28 January 2022; accepted 16 March 2022; published 10 May 2022)

The high-energy γ rays have been measured in proton and α -induced reactions on medium mass target nuclei ^{115}In and ^{112}Sn , respectively. Theoretical analyses of the spectra have been performed within the Hauser-Feshbach statistical model and the Akkermans-Gruppelaar exciton model formalisms. It is observed that the proton-induced reaction has significant contribution from the direct-semidirect capture in the region $E_\gamma \approx 10\text{--}20$ MeV. The ^4He -ion-induced reaction could be described reasonably well by the results of the statistical model calculations. A reduced level density parameter, as compared to that used for the proton-induced reaction, was required to explain the high-energy γ -ray spectrum in the ^4He -ion-induced reaction.

DOI: [10.1103/PhysRevC.105.054602](https://doi.org/10.1103/PhysRevC.105.054602)

I. INTRODUCTION

The γ rays produced during nuclear collisions provide a clean probe to study the reaction dynamics and properties of atomic nucleus. The study of these γ rays has, therefore, been the subject of intense investigations both theoretically and experimentally. In heavy-ion collisions with projectile energies below 7 MeV/nucleon, the reaction mainly proceeds through the two-step compound nuclear mechanism. In such reactions, the γ rays are emitted in competition with particle evaporation, and the spectra are dominated by the giant dipole resonance (GDR) strength function [1–5]. At higher projectile energies (>20 MeV/nucleon), a large yield is observed above $E_\gamma \approx 30$ MeV from the incoherent neutron-proton (n - p) bremsstrahlung process among the target and projectile nucleons [6]. On the other hand, the nucleon-induced reactions show interesting features in the γ -ray spectrum. For projectile energies >50 MeV/nucleon, a large yield is observed above $E_\gamma \approx 30$ MeV, which originates primarily from the incoherent n - p bremsstrahlung process [7]. At low projectile energies, the nucleon may be captured into any of the single-particle configurations of the composite system directly, called direct capture, or through the excitation of the GDR, called semidirect capture [8,9]. The γ rays have significant contribution in the $E_\gamma \approx 10\text{--}30$ MeV region from the direct-semidirect (DSD) mechanism. The γ rays may also be emitted in the two-step compound-capture mechanism in

competition with particle decay. In light mass systems, proton capture reactions have been extensively studied [2,10–14], and the γ -ray spectrum has been explained by the DSD capture mechanism. In the literature, some studies on heavy-mass systems [15–17] are also present. Recently, the GDR properties have been explored in proton capture reactions within the extended quantum molecular dynamics model [18]. Indeed, the proton capture reaction was an important tool to study the giant dipole resonance built on excited states [19–22] before it was shown that heavy-ion reactions could be used to study the same [23]. The DSD mechanism was later extended to the capture of protons to the unbound states [24], and was found to explain the experimental data well. The actual DSD calculation is a bit involved and requires knowledge of the transition matrix element between the states involved in the transition. A powerful method to model the direct-semidirect process is the exciton model calculations. In this formalism, an average transition matrix element is considered, and the γ -ray cross section is calculated in a statistical approach before equilibrium is reached to form the compound nucleus. The first work in this approach was done by Plyuyko and Prokops [25]. Soon after, Běták and Dobeš [26] refined this approach by properly considering the possible γ transitions and accessible final states. The first work consistent with the equilibrium statistical limit was done by Akkermans and Gruppelaar [27] by properly calculating the branching ratios for single-particle transitions contributing in the γ -ray spectra, and later a spin dependent formalism was proposed by Obložinský [28]. Experimentally, these models have not been explored much.

In understanding the decay of an equilibrated compound system, a critical quantity is the nuclear level density (NLD).

*debasishm@vecc.gov.in

†Present address: GSI Helmholtzzentrum für Schwerionenforschung, D-64291 Darmstadt, Germany.

The most widely used level density prescription was derived by Bethe using the noninteracting Fermi gas model [29]. The level density is mainly governed by the NLD parameter which is proportional to the single-particle density of states at the Fermi energy, and is generally expressed as $a = \alpha A$, where α is a constant and A is the mass number of the nucleus. Al-Quraishi *et al.* [30] suggested two alternative forms of the NLD parameter, viz.,

$$a = \frac{\alpha A}{\exp[\beta(N - Z)^2]}, \quad (1)$$

$$a = \frac{\alpha A}{\exp[\gamma(Z - Z_0)^2]}, \quad (2)$$

where α , β , and γ are empirical constants. Z_0 is the atomic number for the β -stable isotope for mass number A . N and Z are the neutron and proton numbers, respectively. Z_0 is obtained from a fit to the semiempirical mass formula [30]. Equation (1) shows that the NLD parameter is maximum for $N = Z = A/2$, and decreases for nuclei having excess protons or neutrons. Equation (2), on the other hand, implies that the NLD parameter decreases for nuclei away from the β -stable isotope. For light mass nuclei ($A \leq 40$), both expressions provide the same results, and deviate for heavy systems. It was shown from the analysis of low-energy level densities that Eq. (2) was better at reproducing the experimental data [30]. Moro *et al.*, on the other hand, showed that the $(N-Z)$ dependence was more appropriate to explain the data obtained in the $^{32}\text{S} + ^{107}\text{Ag}$ compound nuclear reaction [31]. In the work by Charity *et al.* [32], a very small or no effect of isospin on the level density was observed from the measured particle spectra and residues. The theoretical work by Charity and Sobotka [33] also concluded very little dependence of the level density parameter on neutron-proton asymmetry. Only a very small reduction was observed for nuclei close to the drip line. In recent years, light evaporated particles were measured in a few experiments, and a reduced level density parameter was required to explain the experimental data for the nuclei with Z away from Z_0 [34–36].

In this work, we present the results of the measurement of high-energy γ rays in ^1H - and ^4He -ion-induced reactions on medium mass targets ^{115}In and ^{112}Sn [37], respectively, and compare the results with the statistical and exciton model calculations. The target-projectile combinations were chosen so as to populate the nuclei of the same mass number. It is interesting to note that the compound nucleus ^{116}Te populated in the ^4He -ion-induced reaction is ≈ 2 units away from the Z_0 value for $A = 116$, whereas, for ^{116}Sn , $Z \approx Z_0$. In this experiment both the neutrons and high-energy γ rays were measured. The results from the analysis of neutron spectra showed that the level density indeed decreases for neutron-deficient ^{115}Te compared to that of β -stable ^{115}Sn [36], and the $(Z - Z_0)$ dependence was found to be better suited for explaining the experimental data. In this work, the results from the measured high-energy γ rays are presented.

II. EXPERIMENTAL DETAILS

The experiment was performed at the Variable Energy Cyclotron Centre (VECC), Kolkata, India using pulsed ^1H and

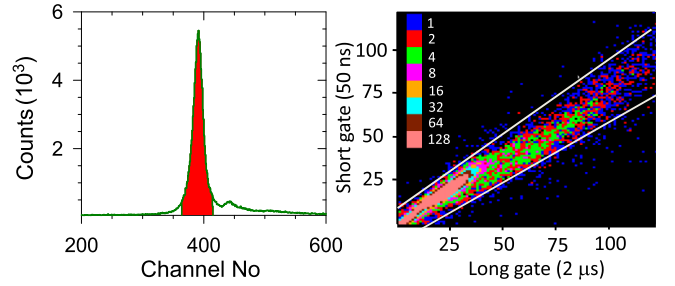


FIG. 1. Typical time-of-flight spectrum (left panel) and pulse shape discrimination spectrum (right panel) along with the cuts used for extraction of high-energy γ -ray spectrum.

^4He -ion beams from the room-temperature K-130 cyclotron. Self-supporting ^{115}In and ^{112}Sn target nuclei were bombarded with ^1H and ^4He -ion beams of energies 12 and 28 MeV, respectively. The maximum available energies in the above-mentioned reactions were 21.2 and 26.1 MeV, respectively. The high-energy γ -rays were detected by using a part of the Large Area Modular BaF_2 Detector Array (LAMBDA) [38]. A total of 49 BaF_2 scintillators, each having cross-sectional area $3.5 \times 3.5 \text{ cm}^2$ and length 35 cm, were arranged in a 7×7 matrix which was placed at a distance of 50 cm from the target position at an angle of 90° with respect to the beam direction. One of the major sources of background in the high-energy γ -ray spectrum is the evaporated neutrons which were rejected by using the time-of-flight (TOF) technique. The start trigger for the TOF measurement was taken from a low-energy γ -ray multiplicity filter [39]. It consists of 50 small BaF_2 scintillators, each having cross-sectional area $3.5 \times 3.5 \text{ cm}^2$ and length 5 cm. The multiplicity filter was divided into two 5×5 arrays of 25 scintillators each, and placed on the top and bottom of the scattering chamber at a distance of $\approx 5 \text{ cm}$ from the target position in a staggered castle type geometry. An event was recorded in a VME based data acquisition system [40] when at least one detector in the LAMBDA array fired above a threshold of $\approx 4 \text{ MeV}$ in coincidence with at least one detector in the multiplicity filter above a threshold $\approx 200 \text{ keV}$. In this sense it is not an inclusive measurement of high-energy γ rays. The pileup events were removed by the pulse shape discrimination technique (PSD) which was achieved by measuring the charge deposition over two time intervals of 2 μs (long gate) and 50 ns (short gate). To block the low-energy γ rays after opening of the high-energy threshold, a passive lead shield was used in front of the LAMBDA array. The beam dump was situated at a distance of $\approx 3 \text{ m}$ from the target, and was heavily shielded with lead and paraffin blocks to minimize the backgrounds. The energy of the γ rays detected in the LAMBDA array was reconstructed by the cluster summing technique [38]. The neutrons were rejected by taking a cut in the γ - γ prompt peak in each detector, whereas the pileup events were rejected with a proper two-dimensional cut in the PSD spectra. Typical TOF and two-dimensional PSD spectra for a detector element of the LAMBDA array are shown in Fig. 1 along with the cuts used in data reconstruction. The high granularity of the LAMBDA array was used to reject the cosmic backgrounds which produce tracks in the array,

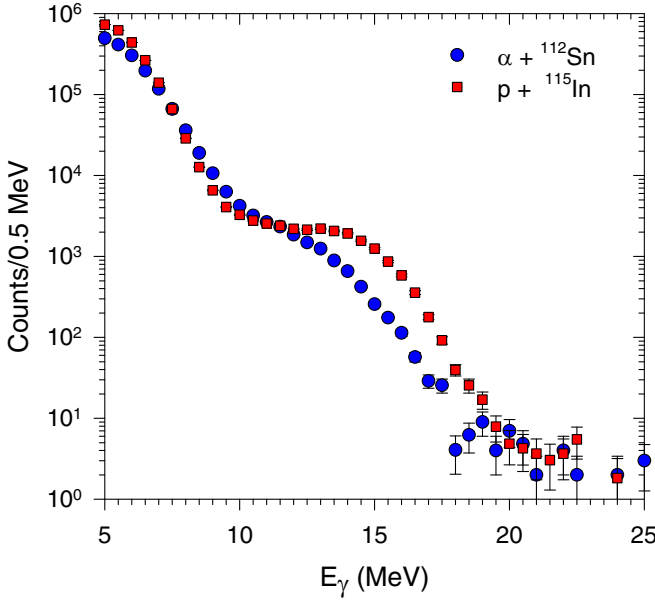


FIG. 2. High-energy γ -ray spectra for the ${}^4\text{He} + {}^{112}\text{Sn}$ (blue filled circles) and ${}^1\text{H} + {}^{115}\text{In}$ reactions (red filled squares).

whereas the actual γ events produce a clusterlike structure. The cyclotron rf time spectrum was also recorded with respect to the multiplicity filter to minimize the random events, and proper cuts were incorporated in the rf time spectrum while reconstructing the high-energy γ -ray spectrum.

In Fig. 2, the high-energy γ -ray spectra are shown for the two reactions. The spectra have been normalized at 7.5 MeV. The γ rays below ≈ 10 MeV arise due to the transitions between the states below particle threshold, and originate primarily from statistical processes. On the other hand, those γ rays above ≈ 10 MeV mainly arise in the initial stages of the reaction. It is interesting to note that the spectra match qualitatively in $E_\gamma \approx 5$ –10 MeV and above the $E_\gamma \approx 20$ MeV region. However, an enhanced yield is observed for the ${}^1\text{H} + {}^{115}\text{In}$ reaction in $E_\gamma \approx 10$ –20 MeV, in comparison to the other reaction, clearly pointing towards different mechanisms in the production of γ rays in this region.

III. THEORETICAL CALCULATIONS

To explain the high-energy γ -ray spectra for the two reactions, we have performed the statistical and the exciton model calculations by using the TALYS-1.95 code [41], which is an excellent tool for calculations at low energies and for light-ion-induced reactions. The statistical model calculations were performed in the Hauser-Feshbach (HF) framework. The transmission coefficients for the particle decay were calculated by using the default options in the TALYS-1.95 code. The γ -ray transmission coefficient was calculated by considering electric and magnetic transitions up to multipolarity $l = 2$. However, it was observed that, apart from the electric dipole transition, the effect of other transitions was negligibly small. The transmission coefficient for the electric dipole transition is given by $T_{E1} = 2\pi f_{E1}(E_\gamma)E_\gamma^3$, where E_γ is the transition energy, and $f_{E1}(E_\gamma)$ is the energy-dependent

dipole strength function calculated by using the Brink-Axel hypothesis [42,43], and is given by

$$f_{E1}(E_\gamma) = \frac{1}{3\pi^2\hbar^2c^2} \frac{\sigma_G(E_\gamma)}{E_\gamma}, \quad (3)$$

where the GDR photoabsorption cross section is given by

$$\sigma_G(E_\gamma) = \frac{\sigma_{G0}E_\gamma^2\Gamma_G^2}{(E_\gamma^2 - E_G^2)^2 + E_\gamma^2\Gamma_G^2}, \quad (4)$$

where σ_{G0} , Γ_G , and E_G are the strength, width, and energy of the giant dipole resonance, respectively. The strength is given by $\sigma_{G0} = S_G[120(NZ/A)(1/\pi\Gamma_G)]$ mb, S_G being the fraction of the Thomas-Reiche-Kuhn (TRK) dipole sum rule strength. Another important quantity for the statistical model calculations is the nuclear level density. In the present work the back-shifted Fermi gas (BFG) level density prescription was employed. According to this prescription the level density at an excitation energy E_x and angular momentum J is given by

$$\rho(E_x, J) = \frac{2J+1}{2\sigma^2} \exp\left[-\frac{(J+\frac{1}{2})^2}{2\sigma^2}\right] \rho_f^t(E_x), \quad (5)$$

where σ^2 is the spin cut-off parameter and $\rho_f^t(E_x)$ is the total Fermi gas level density at excitation energy E_x given by

$$\rho_f^t(E_x) = \frac{1}{\sqrt{2\pi}\sigma} \frac{\sqrt{\pi} \exp[2\sqrt{aU}]}{12 a^{\frac{1}{4}} U^{\frac{5}{4}}}, \quad (6)$$

where $U = E_x - \Delta$, Δ being the energy back-shift given by $\Delta = \chi \frac{12}{\sqrt{A}} + \delta$. $\chi = 1, 0$, and -1 for even-even, odd-even, and odd-odd nuclei, respectively. δ is an adjustable parameter to fit the experimental data per nucleus. The shell effect was incorporated in the level density parameter by the prescription of Ignatyuk *et al.* and is given by $a(E_x) = \tilde{a}[1 + \frac{\Delta S}{U}\{1 - \exp(-\gamma U)\}]$ [44]. Here ΔS is the ground state shell correction, and γ is the shell damping factor given by $\gamma = \frac{\gamma_1}{A^{1/3}}$. γ_1 was chosen so as to reproduce $\gamma \approx 0.06$ MeV $^{-1}$ in the Pb region, reported earlier [45]. In the TALYS code the asymptotic level density parameter is expressed as $\tilde{a} = \alpha A + \beta A^{2/3}$, and $\alpha = 0.0722396$ and $\beta = 0.195267$ are used globally for the back-shifted Fermi gas model. In the present case we have used the linear term, i.e., $\tilde{a} = \alpha A$ with α as a free parameter to match the experimental data.

Within the TALYS code, the formalism of Akkermans and Gruppelaar [27] was implemented to calculate the γ -ray emission cross section in the exciton model framework. It provides a powerful tool to calculate γ -ray cross section in the direct-semidirect process. Within this model, the preequilibrium γ -ray cross section is given by

$$\frac{d\sigma_\gamma}{dE_\gamma} = \sigma_{\text{cf}} \sum_n W_\gamma(n, E_\gamma) \tau(n), \quad (7)$$

where the composite nucleus formation cross section with the target and projectile is calculated as $\sigma_{\text{cf}} = \sigma_{\text{tot}} - \sigma_{\text{direct}}$. σ_{tot} and σ_{direct} are the total and direct reaction cross sections, respectively. $\tau(n)$ is the mean lifetime and $W_\gamma(n, E_\gamma)$ is the decay rate from the exciton state n for a γ ray of energy E_γ . It

is calculated by using the principle of detailed balance, and is given by

$$W_\gamma(n, E_\gamma) = \frac{E_\gamma^2}{\pi^2 \hbar^3 c^2} \sigma_{\text{abs}}(E_\gamma) \frac{1}{\omega_n(E)} \times \left[\frac{\omega_2(E_\gamma) \omega_{n-2}(E - E_\gamma)}{g(n-2) + \omega_2(E_\gamma)} + \frac{g n \omega_n(E - E_\gamma)}{g n + \omega_2(E_\gamma)} \right], \quad (8)$$

where $\omega_n(E)$ is the density of exciton state n at excitation energy E , and g is the single-particle state density. The photoabsorption cross section is given by $\sigma_{\text{abs}}(E_\gamma) = \sigma_G(E_\gamma) + \sigma_{\text{QD}}(E_\gamma)$, where $\sigma_{\text{QD}}(E_\gamma)$ is the quasi-deuteron part of the photoabsorption cross section. Generally, it contributes at higher γ ray energies, and has negligible contribution in the present case. It should be pointed out that the exciton model of Akkermans and Gruppelaar, in principle, can calculate the pre-equilibrium as well as equilibrium γ -ray cross sections in a consistent way. However, in the TALYS code the pre-equilibrium phase is calculated by using the exciton model, whereas the equilibrium phase is calculated by employing the usual Hauser-Feshbach formalism. We remark here that the two-component exciton model was used in this work, where the proton and neutron excitons are considered separately. The detailed expressions for the decay rates and γ -decay cross section in the two-component exciton model can be found in the manual of the TALYS code.

IV. RESULTS AND DISCUSSION

In Fig. 3, the experimental high-energy γ -ray spectrum for the $^1\text{H} + ^{115}\text{In}$ reaction is shown along with the results of the statistical and exciton model calculations. Before comparison with the measured spectrum, the theoretically calculated spectra were folded with the detector response function simulated by using the GEANT3 [46] code. The theoretical spectra folded with the detector response function have been normalized at $E_\gamma \approx 7.5$ MeV with the experimentally measured spectrum. As could be observed from Fig. 3(a), the result of the statistical model calculation highly underpredicts the measured data for $E_\gamma > 10$ MeV. However, when the preequilibrium contribution calculated by employing the exciton model was added with that obtained from the HF calculations, the experimental spectrum could be explained well. It should be highlighted here that the HF and the exciton model calculations were performed by employing the same set of the GDR parameters. Apart from that, the exciton model calculation was performed with all the default parameters used in the TALYS code. We remark here that, to match the data, the contribution from the exciton model calculations had to be reduced to 14% of the total contribution above $E_\gamma \approx 16.5$ MeV. This could be due to the fact that the high-energy γ rays were detected in coincidence with at least one detector of the multiplicity filter. However, this reduction does not affect the spectra in the $E_\gamma \approx 10$ –16 MeV region where a substantial enhanced yield is observed compared to that of the statistical model calculations. In Fig. 3(b), the experimental high-energy γ -ray spectrum is shown along with the results of the theoretical calculations with the total and the reduced contributions in

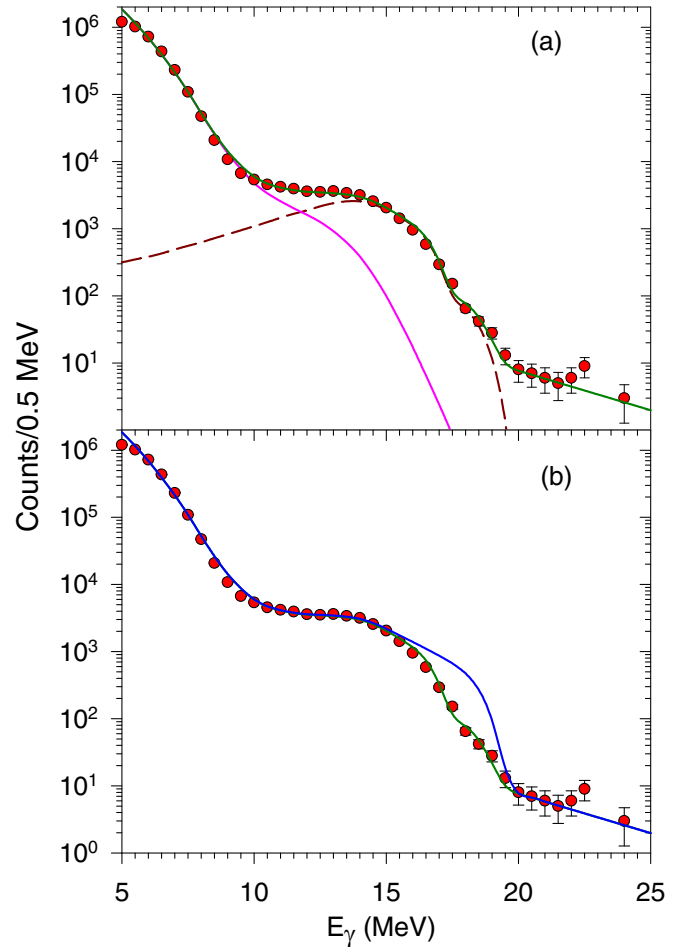


FIG. 3. (a) Experimental high-energy γ -ray spectrum (red filled circles) for the $^1\text{H} + ^{115}\text{In}$ reaction along with the results of the statistical (pink solid line) and exciton (dark red dashed line) model calculations. (b) Effects of the total (blue solid line) and reduced (green solid line) contributions in the exciton model calculation are shown (see the text).

the exciton model calculations. In the HF calculations the equivalent value of the parameter α is ≈ 0.1123 MeV $^{-1}$. However, the spectrum below $E_\gamma \approx 10$ MeV could be fitted reasonably better when the value of α was increased slightly to ≈ 0.1135 MeV $^{-1}$. The γ -ray spectra calculated within the HF and the exciton models were not normalized individually. The spectra were added and then the added spectrum was normalized at 7.5 MeV. It should be pointed out that in the TALYS code an extra normalization of 2.0 is provided by default in the calculation of photon emission rate within the exciton model. Above $E_\gamma \approx 20$ MeV there may be contribution from the n - p bremsstrahlung process, which has been parametrized as $\sigma = \sigma_0 \exp(-E_\gamma/E_0)$ [6,7]. The parameters σ_0 and E_0 were chosen to fit the data above $E_\gamma \approx 20$ MeV. In Table I the best-fit parameters are shown.

In Fig. 4, the experimental high-energy γ -ray spectrum for the $^4\text{He} + ^{112}\text{Sn}$ reaction is shown along with the results of the statistical model calculations. Figs. 4(b) and 4(d) represent the divided plots which prominently show the effects of the GDR parameters on the high-energy γ -ray spectra.

TABLE I. The GDR and other parameters required to fit the high-energy γ -ray spectra for the reactions mentioned.

Reaction	E_G (MeV)	Γ_G (MeV)	S_G	α (MeV $^{-1}$)	E_0 (MeV)	σ_0 (arb. units)
$^1\text{H} + ^{115}\text{In}$	14.0(1)	4.0(2)	1.00(4)	0.1135(3)	3.7(1)	$1.7(4) \times 10^3$
$^4\text{He} + ^{112}\text{Sn}$	14.1(1)	4.7(2)	1.02(4)	0.0890(4)	3.0(2)	$3.5(9) \times 10^3$

These plots were obtained by dividing both the experimental and the best-fit γ -ray spectra by a γ -ray spectrum calculated with a constant dipole strength function without incorporating the GDR. The contribution of high-energy γ rays from the preequilibrium process was found to be negligibly small. It is interesting to note that the parameters which were used for the statistical model calculations in the $^1\text{H} + ^{115}\text{In}$ reaction could not describe the high-energy γ -ray spectrum for the $^4\text{He} + ^{112}\text{Sn}$ reaction [blue dashed line in Figs. 4(a) and 4(b)] even after incorporating the pre-equilibrium contribution. The data could be fitted by varying the GDR parameters with the level density parameter, as used for the statistical model calculations in the $^1\text{H} + ^{115}\text{In}$ reaction. In this case, the GDR energy and width were found to be 14.6 and 4.7 MeV, respectively. However, an extra strength of $\approx 50\%$ more than that obtained from the TRK sum rule was required. Interestingly, the data could be reproduced quite well [Figs. 4(c) and 4(d)] with the strength of $\approx 100\%$ as obtained from the TRK sum rule, and reasonable GDR energy and width, when a reduced level density was utilized by decreasing the value of α (Table I) by $\approx 21\%$ compared to that used for describing the proton-induced reaction. We remark here that, at the excitation energy considered in the present case, the high-energy γ rays ($E_\gamma \approx 10$ – 20 MeV) originate primarily

from the decay of the GDR of the compound nucleus ^{116}Te . The proton number of this nucleus is ≈ 2 units away from the Z_0 value for $A = 116$. The contribution from the daughter nuclei is very small. Moreover, the average value of $(Z - Z_0)^2$ for the nuclei in the decay cascade of ^{116}Te is large compared to that for the nuclei in the decay cascade of ^{116}Sn . Therefore, it is expected that the level density for the nuclei with Z away from Z_0 is decreased as suggested in Ref. [30], and experimentally confirmed in earlier works [34,36]. For example, with the parameters used in the present work, the total level density for the ^{116}Te nucleus is of ≈ 9 times smaller than that of the β -stable ^{116}Sn nucleus at the excitation energy of ≈ 10 MeV.

It should be mentioned that we tried to explain the measured γ -ray spectra by using the Gilbert-Cameron formulation for the level density [47]. However, in this case, the slope of the γ -ray spectrum below $E_\gamma \approx 10$ MeV for the $^1\text{H} + ^{115}\text{In}$ reaction could not be reproduced well with the default level density parameters used in the TALYS code. The fit could not be improved with a reasonable variation of the parameter α . In addition to the phenomenological models, we tried to reproduce the measured γ -ray spectra by utilizing the microscopic prescriptions implemented in the TALYS-1.95 code. The γ -ray spectrum for the $^1\text{H} + ^{115}\text{In}$ reaction could be explained best by using the level densities from Hilaire's combinatorial tables [48]. In this microscopic approach, nuclear level density is computed by a combinatorial method where the incoherent particle-hole state densities are calculated as a function of excitation energy, spin projection, and parity by using the Hartree-Fock-Bogoliubov single-particle level scheme, and the total level density is calculated by properly taking into account the collective effects. The GDR parameters were found to be $E_G \approx 13.6$ MeV (which is a bit smaller than that expected in this mass region), $\Gamma_G \approx 4.0$ MeV, and $S_G \approx 1.03$. Interestingly, when the same microscopic prescription was utilized to explain the γ -ray spectrum for the $^4\text{He} + ^{112}\text{Sn}$ reaction, the GDR parameters were found to be $E_G \approx 14.2$ MeV, $\Gamma_G \approx 4.8$ MeV, and $S_G \approx 1.58$, i.e., an extra strength of $\approx 58\%$ more than that obtained from the TRK sum rule was required, which is roughly similar to that observed for the phenomenological BFG model. The high-energy γ -ray spectra for both the reactions could be explained in the whole region with the most reasonable GDR parameters by using the BFG model, which points towards the reduction of the level density for ^{116}Te as compared to that of the ^{116}Sn . This reduction in the level density may have crucial implications for the reaction model calculations involving the proton-rich and the neutron-rich nuclei. Further studies are required with both the proton-rich and neutron-rich isotopes for a better understanding of the level densities for such systems.

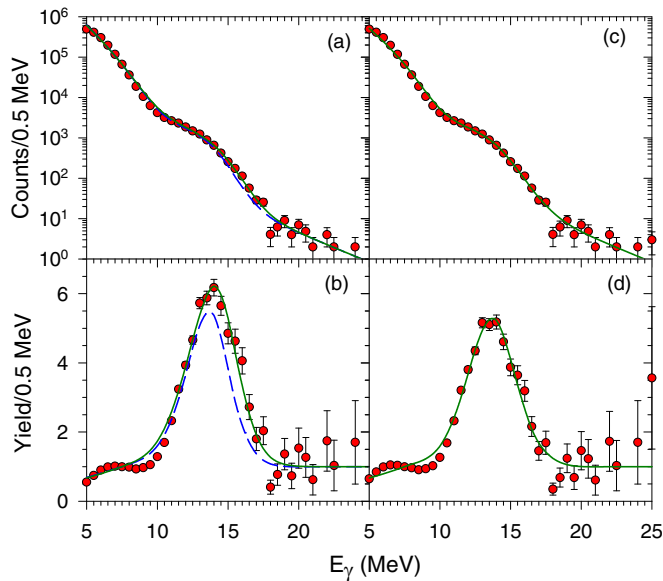


FIG. 4. (a) and (c) Experimental high-energy γ -ray spectra for the $^4\text{He} + ^{112}\text{Sn}$ reaction (red filled circles) along with the results of the statistical model calculations (lines). (b) and (d) The experimental spectra and statistical model calculations with the GDR, divided by the respective results of the statistical model calculations with a constant dipole strength without the GDR.

V. SUMMARY AND CONCLUSION

In summary, the high-energy γ -ray spectra have been measured in the $^1\text{H} + ^{115}\text{In}$ and $^4\text{He} + ^{112}\text{Sn}$ reactions. The proton-induced reaction shows a large yield in the GDR region arising due to the direct-semidirect capture process. The data could be well explained by considering both the contributions from the Hauser-Feshbach and exciton model calculations. The α -induced reaction, on the other hand, shows minimal contribution from the direct-semidirect capture mechanism, and the experimental data could be well explained by the statistical HF-model calculations. The level density of neutron-deficient ^{116}Te is found to be reduced as compared to that of β -stable ^{116}Sn . Considering the profound importance of the level density for reaction studies, it will be interesting and essential to have more experimental and

theoretical works in different regions of the nuclear chart for a better understanding of the isospin dependence of nuclear level density.

ACKNOWLEDGMENTS

The authors are thankful to the VECC cyclotron staff for smooth running of the accelerator during the experiment. The authors thank H. Pai for providing the ^{112}Sn target, and Ruchismita Mondal Saha for preparing the ^{115}In target. D.M. acknowledges email conversations with Prof. A. J. Koning. S.R.B. acknowledges the financial assistance from the Science and Engineering Research Board, Government of India, Grant No. CRG-2018-000336.

-
- [1] M. N. Harakeh and A. van der Woude, *Giant Resonances: Fundamental High-Frequency Mode of Nuclear Excitation* (Clarendon, Oxford, 2001).
- [2] K. A. Snover, *Annu. Rev. Nucl. Part. Sci.* **36**, 545 (1986).
- [3] J. J. Gaardhoje, *Annu. Rev. Nucl. Part. Sci.* **42**, 483 (1992).
- [4] A. Schiller *et al.*, *At. Data Nucl. Data Tables* **93**, 549 (2007).
- [5] D. R. Chakrabarty *et al.*, *Eur. Phys. J. A* **52**, 143 (2016).
- [6] W. Cassing *et al.*, *Phys. Rep.* **188**, 363 (1990).
- [7] H. Nifenecker and J. A. Pinston, *Annu. Rev. Nucl. Part. Sci.* **40**, 113 (1990).
- [8] A. M. Lane, *Nucl. Phys.* **11**, 625 (1959).
- [9] G. E. Brown, *Nucl. Phys.* **57**, 339 (1964).
- [10] E. M. Diener, J. F. Amann, and P. Paul, *Phys. Rev. C* **7**, 695 (1973).
- [11] K. A. Snover, P. Paul, and H. M. Kuan, *Nucl. Phys. A* **285**, 189 (1977).
- [12] M. A. Kovash, S. L. Blatt, R. N. Boyd, T. R. Donoghue, H. J. Hausman, and A. D. Bacher, *Phys. Rev. Lett.* **42**, 700 (1979).
- [13] H. R. Weller, H. Hasan, S. Manglos, G. Mitev, N. R. Roberson, S. L. Blatt, H. J. Hausman, R. G. Seyler, R. N. Boyd, T. R. Donoghue, M. A. Kovash, A. D. Bacher, and C. C. Foster, *Phys. Rev. C* **25**, 2921 (1982).
- [14] H. J. Hausman, S. L. Blatt, T. R. Donoghue, J. Kalen, W. Kim, D. G. Marchlinski, T. W. Rackers, P. Schmalbrock, M. A. Kovash, and A. D. Bacher, *Phys. Rev. C* **37**, 503 (1988).
- [15] P. J. Daly and P. F. D. Shaw, *Nucl. Phys.* **56**, 322 (1964).
- [16] B. Pålsson *et al.*, *Nucl. Phys. A* **345**, 221 (1980).
- [17] D. R. Chakrabarty, V. M. Datar, Y. K. Agarwal, C. V. K. Baba, M. S. Samant, I. Mazumdar, A. K. Sinha, and P. Sugathan, *Phys. Rev. C* **60**, 024606 (1999).
- [18] K. Wang, Y. G. Ma, G. Q. Zhang, X. G. Cao, W. B. He, and W. Q. Shen, *Phys. Rev. C* **95**, 014608 (2017).
- [19] P. P. Singh *et al.*, *Nucl. Phys.* **65**, 577 (1965).
- [20] H. F. Glavish *et al.*, *Phys. Rev. Lett.* **28**, 766 (1972).
- [21] G. A. Fisher *et al.*, *Phys. Rev. C* **14**, 28 (1976).
- [22] D. H. Dowell, G. Feldman, K. A. Snover, A. M. Sandorfi, and M. T. Collins, *Phys. Rev. Lett.* **50**, 1191 (1983).
- [23] J. O. Newton, B. Herskind, R. M. Diamond, E. L. Dines, J. E. Draper, K. H. Lindenberger, C. Schuck, S. Shih, and F. S. Stephens, *Phys. Rev. Lett.* **46**, 1383 (1981).
- [24] W. E. Parker, M. B. Chadwick, F. S. Dietrich, J. E. Kammeraad, S. J. Luke, K. E. Sale, R. M. Chasteler, M. A. Godwin, L. H. Kramer, G. J. Schmid, H. R. Weller, and A. K. Kerman, *Phys. Rev. C* **52**, 252 (1995).
- [25] V. A. Plyuyko and G. A. Prokopets, *Phys. Lett. B* **76**, 253 (1978).
- [26] E. Běták and J. Dobeš, *Phys. Lett. B* **84**, 368 (1979).
- [27] J. M. Akkermans and H. Gruppelaar, *Phys. Lett. B* **157**, 95 (1985).
- [28] P. Obložinský, *Phys. Rev. C* **35**, 407 (1987).
- [29] H. A. Bethe, *Phys. Rev.* **50**, 332 (1936); *Rev. Mod. Phys.* **9**, 69 (1937).
- [30] S. I. Al-Quraishi, S. M. Grimes, T. N. Massey, and D. A. Resler, *Phys. Rev. C* **63**, 065803 (2001).
- [31] R. Moro *et al.*, *Eur. Phys. J. A* **48**, 159 (2012).
- [32] R. J. Charity, L. G. Sobotka, J. F. Dempsey, M. Devlin, S. Komarov, D. G. Sarantites, A. L. Caraley, R. T. deSouza, W. Loveland, D. Peterson, B. B. Back, C. N. Davids, and D. Seweryniak, *Phys. Rev. C* **67**, 044611 (2003).
- [33] R. J. Charity and L. G. Sobotka, *Phys. Rev. C* **71**, 024310 (2005).
- [34] A. V. Voinov, T. Renstrom, D. L. Bleuel, S. M. Grimes, M. Guttormsen, A. C. Larsen, S. N. Liddick, G. Perdikakis, A. Spyrou, S. Akhtar, N. Alanazi, K. Brandenburg, C. R. Brune, T. W. Danley, S. Dhakal, P. Gastis, R. Giri, T. N. Massey, Z. Meisel, S. Nikas *et al.*, *Phys. Rev. C* **99**, 054609 (2019).
- [35] G. K. Prajapati, Y. K. Gupta, B. V. John, B. N. Joshi, H. Kaur, N. Kumar, L. S. Danu, S. Mukhopadhyay, S. Dubey, S. R. Jain, D. C. Biswas, and B. K. Nayak, *Phys. Rev. C* **102**, 054605 (2020).
- [36] P. Roy, K. Banerjee, T. K. Rana, S. Kundu, S. Manna, A. Sen, D. Mondal, J. Sadhukhan, M. T. Senthil Kannan, T. K. Ghosh, S. Mukhopadhyay, D. Pandit, G. Mukherjee, S. Pal, D. Paul, K. Atreya, and C. Bhattacharya, *Phys. Rev. C* **102**, 061601(R) (2020).
- [37] H. Pai *et al.*, *Vacuum* **167**, 393 (2019).
- [38] S. Mukhopadhyay *et al.*, *Nucl. Instrum. Methods Phys. Res., Sect. A* **582**, 603 (2007).

- [39] D. Pandit *et al.*, [Nucl. Instrum. Methods Phys. Res., Sect. A](#) **624**, 148 (2010).
- [40] P. Dhara *et al.*, Proc. DAE-BRNS Symp. Nucl. Phys. **50**, 454 (2005).
- [41] A. J. Koning *et al.*, TALYS-1.95, www.talys.eu.
- [42] D. M. Brink, Ph.D. thesis, University of Oxford, 1955 (unpublished).
- [43] P. Axel, [Phys. Rev.](#) **126**, 671 (1962).
- [44] A. V. Ignatyuk *et al.*, [Yad. Fiz.](#) **21**, 485 (1975) [[Sov. J. Nucl. Phys.](#) **21**, 255 (1975)].
- [45] P. C. Rout, D. R. Chakrabarty, V. M. Datar, S. Kumar, E. T. Mirgule, A. Mitra, V. Nanal, S. P. Behera, and V. Singh, [Phys. Rev. Lett.](#) **110**, 062501 (2013).
- [46] R. Brun *et al.*, GEANT3, Report No. CERN-DD/EE/84-1, 1986 (unpublished).
- [47] A. Gilbert and A. G. W. Cameron, [Can. J. Phys.](#) **43**, 1446 (1965).
- [48] S. Goriely, S. Hilaire, and A. J. Koning, [Phys. Rev. C](#) **78**, 064307 (2008).